Growth, characterization and interfacial reaction of magnetron sputtered Pt/CeO_2 thin films on Si and Si_3N_4 substrates

C. Anandan and Parthasarathi Bera*

Surface Engineering Division, CSIR–National Aerospace Laboratories, Bangalore 560017, India

Abstract

Pt/CeO_2 thin films were deposited on Si and Si_3N_4 substrates by magnetron sputtering at room temperature. Growth of the films on Si and Si_3N_4 were characterized by XRD, FESEM and AFM. Interaction of Pt/CeO_2 films with Si in Si and Si_3N_4 substrates was extensively investigated by XPS. XRD studies show that films are oriented preferentially to (200) direction of CeO_2. XPS results show that Pt is mainly present in +2 oxidation state in $Pt/CeO_2/Si$ film, whereas Pt^{4+} predominates in $Pt/CeO_2/Si_3N_4$ film. Ce is present as both +4 and +3 oxidation states in Pt/CeO_2 films deposited on both Si and Si_3N_4 substrates, but concentration of Ce^{3+} species is observed to be more in $Pt/CeO_2/Si$ film. Interfacial reaction between CeO_2 and Si substrate is controlled in presence of Pt. Pt/Ce concentration ratio decreases in $Pt/CeO_2/Si_3N_4$ film upon successive sputtering, whereas this ratio decreases initially and then increases in $Pt/CeO_2/Si$ film. Pt is segregated at the interface in $Pt/CeO_2/Si$ film, whereas Pt is diffused outwards in $Pt/CeO_2/Si_3N_4$ film as observed from depth profiling studies.

Keywords: Thin films; Pt/CeO_2; Si and Si_3N_4 substrates; Interfacial reaction; XPS

---

*Corresponding author

Tel: +91–80–25086359, Fax: +91–80–25210113, E mail: partho@nal.res.in

1. Introduction

Metal oxides are an important class of materials due to their potential applications in heterogeneous catalysis, photocatalysis, electrochemistry, sensors, solar cells and electronic devices [1–10]. Addition of a second metal into metal oxide matrix forming a mixed metal/metal oxide interface can exhibit interesting properties that are fundamentally different from those of respective metal oxides. In this sense, detailed understanding of metal/metal oxide interface is very crucial from fundamental view point.

CeO_2 has been extensively studied due to its various applications in last several years. It is an attractive material for various catalytic, electronic, optical, electrical, electrochemical, gas sensor and corrosion resistant applications [11–19]. In recent years, Pt/CeO_2 catalyst has widely been used in auto exhaust and fuel cell catalysis for its high activity [20,21]. Catalytic activity of Pt/CeO_2 is influenced by redox nature of CeO_2 as well as the synergistic effect between Pt and CeO_2. Pt/CeO_2 thin films show significant catalytic activity towards methanol electrooxidation and high activity in polymer electrolyte membrane fuel cell (PEMFC) as anode material [22]. Matolín et al. have demonstrated the presence of Pt^{2+} species in Pt/CeO_2 thin film grown on Si substrate, whereas both Pt^{2+} and Pt^{4+} species are observed in the same film grown on carbon nanotube [23]. This suggests that substrates influence the oxidation states and concentration of Pt species.

Pt/CeO_2 thin films have mainly been grown on Si, carbon nanotube, graphite foil, glassy carbon and glass substrates [22–28]. Significant works on the growth, structure and interfacial reaction between CeO_2 and different substrates have been in the literature [29–32]. Recently, we have investigated interfacial reactions between CeO_2 and substrates like Si, Al, Ti–6Al–4V alloy, Si_3N_4 and glass using XPS [30,31]. However, detailed studies on the nature of interaction

between Pt/CeO_2 thin film and different substrates and its influence on the electronic structure are limited in the literature. Moreover, growth and structure of Pt/CeO_2 on Si_3N_4 substrate and their interaction lack in the literature. In the present study, we report the growth of Pt/CeO_2 films on Si and Si_3N_4 substrates by magnetron sputtering. Structure, morphology and roughness of Pt/CeO_2 films are investigated by X-ray diffraction (XRD), field emission scanning electron microscopy (FESEM) and atomic force microscopy (AFM), respectively. X-ray photoelectron spectroscopy (XPS) studies have been carried out in details to understand the interfacial reaction between Pt/CeO_2 thin films and substrates.

2. Experimental methods

Pt/CeO_2 thin films were deposited on Si and Si_3N_4 substrates using a CeO_2 target (Allvac, 99.9%) and Pt foil (Arora Matthey, 99.9%) employing magnetron sputtering assisted by inductively coupled plasma generated with 50 W radio frequency (RF) power at 13.56 MHz. Pt foil was kept on the middle of the CeO_2 target. The substrates were cleaned with acetone/isopropyl alcohol by sonication prior to loading into the vacuum chamber. The chamber was pumped down to a base pressure of 3×10^{-6} mbar. The substrates were etched with H_2 plasma prior to deposition of thin films. Sputter deposition was carried out at room temperature with Ar atmosphere at a pressure of 8 μbar. The substrate was biased to a constant negative voltage of 150 V, whereas the target was biased with bipolar pulses of 300 V using a pulse generator. Thickness of obtained Pt/CeO_2 thin films is 25 ± 1 nm.

The structure of Pt/CeO_2 films was determined by XRD employing a PANalytical X'Pert PRO X-Ray diffractometer operated with CuKα radiation of 1.5418 Å wavelength at 40 kV and 30 mA in the 2θ range 20−80° in bulk mode. The surface morphology of thin films were examined by FESEM using a Carl Zeiss Supra 40. Detailed surface roughness was investigated

by AFM from CSEM Instruments (Model SSI) operated in non-contact mode. XPS of Pt/CeO_2 thin films were recorded with a SPECS spectrometer using non-monochromatic AlKα radiation (1486.6 eV) as an X-ray source operated at 150 W (12.5 kV and 12 mA). The binding energies reported here were calculated with reference to C1s peak at 284.6 eV. All the spectra were obtained with pass energy of 25 eV and step increment of 0.05 eV. Successive sputtering was carried out by defocused Ar^+ ion beam using QE11/35 ion gun by applying energy of 1 keV with Ar gas pressure of 2×10^{-6} Torr for 3, 5, 5, 5, 5 and 5 min. Depth profile spectra were recorded with pass energy of 40 eV and step increment of 0.05 eV. The experimental data were curve fitted into several components with Gaussian–Lorentzian peaks after Shirley background subtraction employing CasaXPS program.

3. Results and discussion

Structural and morphological studies

XRD patterns of Pt/CeO_2 films deposited on Si and Si_3N_4 are shown in the range of 20–60° in Fig. 1. A broad peak at 33.2° noticed in both the films is indexed into CeO_2(200) reflection indicating the nanocrystalline nature of the films [33,34]. Presence of only (200) diffraction peak in $Pt/CeO_2/Si$ film indicates that the film structure on Si substrate is orientated preferentially to (200) plane of CeO_2. On the other hand, in Pt/CeO_2 film deposited on Si_3N_4, low intense peaks at 28.5°, 47.5° and 56.3° associated with reflections from (111), (220) and (311) planes of CeO_2 are also observed along with intense peak at 33.2°. It is to be noted that peaks related to Pt metal, PtO or PtO_2 cannot be detected in both the films indicating that Pt is incorporated as ions into CeO_2 lattice which agrees well with works on Pt/CeO_2 catalysts done by Bera et al [20]. Grain sizes calculated from Debye-Scherrer method are 4.5 and 4.3 nm for $Pt/CeO_2/Si$ and $Pt/CeO_2/Si_3N_4$, respectively.

Fig. 2 displays FESEM images of as-deposited Pt/CeO_2 films on Si and Si_3N_4 substrates. Micrographs show that obtained films have good adherence to the substrates. The surface of Pt/CeO_2 film deposited on Si substrate is very smooth and composed of very fine grains, whereas film coated on Si_3N_4 shows uniform morphology with large grain size. This can be due to the difference in roughness of the substrates.

Surface roughness of Pt/CeO_2 films has been obtained by AFM. The 3D AFM images of as-deposited Pt/CeO_2 thin films deposited on Si and Si_3N_4 substrates are shown in Fig. 3. Average roughness (R_a) and root mean square roughness (R_{rms}) values for $Pt/CeO_2/Si$ are 0.35 and 0.48 nm, whereas those for $Pt/CeO_2/Si_3N_4$ are 3.53 and 4.47 nm, respectively. It can be seen that roughness of Pt/CeO_2 film on Si_3N_4 is more in comparison with that on Si substrate in as-deposited condition that can be due to the higher roughness of Si_3N_4 substrate.

XPS studies

Detailed XPS studies of Pt/CeO_2 thin films deposited on Si and Si_3N_4 substrates have been carried out to understand the interfacial reaction between Pt/CeO_2 films and these substrates. XPS of $Pt/CeO_2/Si$ and $Pt/CeO_2/Si_3N_4$ films with Pt concentrations of 7 and 9 at.%, respectively are discussed here.

Pt4f core level spectra

XPS of Pt 4f core level in Pt/CeO_2 thin films deposited on Si and Si_3N_4 substrates are observed to be broad in nature indicating the presence of multiple oxidation states of Pt. In both $Pt/CeO_2/Si$ and $Pt/CeO_2/Si_3N_4$ films, Pt4f spectra are resolved into sets of spin-orbit doublets and their curve fitted spectra are shown in Fig. 4. Accordingly, $Pt4f_{7/2,5/2}$ peaks at 72.2, 75.5 and 74.4, 77.7 eV observed in $Pt/CeO_2/Si$ thin film are assigned to Pt^{2+} and Pt^{4+}, respectively [20,23]. Peaks at similar binding energies are also observed in $Pt/CeO_2/Si_3N_4$ film. However,

concentration of Pt^{2+} is observed to be more in the film deposited on Si substrate in relation to Si_3N_4 substrate. In $Pt/CeO_2/Si$ film, concentration of Pt^{2+} is 88%, whereas it is 47% in case of $Pt/CeO_2/Si_3N_4$ film. It is important to note that Pt metal peak is not observed in both the films indicating the Pt–CeO_2 interaction. This interaction results in the incorporation of Pt into Ce^{4+} sites in CeO_2 lattice as ions that agrees well the XRD studies demonstrating the absence of Pt metal peaks. Incorporation of Pt, Ru and In into CeO_2 has been reported in the literature [20,34–36]. Matolín et al. have shown the presence of different amount of Pt^{2+} and Pt^{4+} in Pt/CeO_2 thin films deposited on different substrates [23–25,27].

Ce3d core level spectra

Spectral nature of the Pt/CeO_2 film deposited on Si and Si_3N_4 substrates indicate that Ce is in both +4 and +3 oxidation states and it can be resolved into several $Ce3d_{5/2,3/2}$ spin-orbit doublet peaks. In Fig. 5, curve fitted Ce3d core level spectra of Pt/CeO_2 thin films coated on Si and Si_3N_4 substrates are presented. In these figures, peaks labeled as v correspond to $3d_{5/2}$ photoemissions, whereas u peaks are related to $3d_{3/2}$ photoemissions. In Ce3d spectrum of $Pt/CeO_2/Si$ film of Fig. 5, v′′′ and u′′′ spin-orbit peaks at 897.9 and 916.4 eV, respectively with 18.5 eV separation are assigned for the primary photoionization from Ce^{4+} with $Ce3d^94f^0O2p^6$ final state. Lower binding energy states of v′′–u′′ (888.5 and 907.0 eV) and v–u (882.5 and 900.9 eV) have been assigned to the shake-down satellite features of $Ce3d^94f^1O2p^5$ and $Ce3d^94f^2O2p^4$ final states, respectively [37–39]. Satellite peaks are associated with the charge transfer from ligand (O2p) to metal (Ce4f) during primary photoionization processes. Peaks labeled as v_o, u_o and v′, u′ at 881.7, 899.1 and 885.3, 903.4 eV, respectively are associated with Ce^{3+} final states. It is to be noted that v′–u′ spin orbit doublet peaks correspond to main photoionization from $Ce3d^94f^1O2p^6$ final state, whereas lower binding energy v_o–u_o peaks are attributed to

characteristic shake-down satellites of $Ce3d^94f^2O2p^5$ final state [38–40]. It is clear from Fig. 5 that the intensities of Ce^{4+} and Ce^{3+} peaks for Pt/CeO_2 film deposited on Si_3N_4 substrate are different from $Pt/CeO_2/Si$ film. Binding energies and relative integrated peak areas of $Ce3d_{5/2,3/2}$ spin-orbit doublets in Pt/CeO_2 films deposited on Si and Si_3N_4 substrates are summarized in Tables 1 and 2, respectively. Peak areas of Ce^{4+} and Ce^{3+} components are commonly used to estimate their relative concentrations in the films. Concentration of Ce^{4+} in Pt/CeO_2 deposited on Si is estimated to be 77% with respect to the total amount of Ce species indicating the presence of significant amount of Ce^{3+} species. On the other hand, concentration of Ce^{4+} is 83% in Pt/CeO_2 deposited on Si_3N_4 substrate. However, amount of Ce^{3+} is less in $Pt/CeO_2/Si$ film in the present study compared to CeO_2/Si film as demonstrated by our earlier work, whereas Ce^{3+} concentration is more in $Pt/CeO_2/Si_3N_4$ film in relation to CeO_2/Si_3N_4 [30]. Concentrations of Ce^{4+} and Ce^{3+} in Pt/CeO_2 and CeO_2 films deposited on Si and Si_3N_4 substrates are given in Table 3. It has been shown in our previous study that there is a limited interfacial reaction between CeO_2 and Si when CeO_2 is deposited on Si_3N_4 substrate [30]. In the present work, lower concentration of Ce^{3+} in $Pt/CeO_2/Si$ film compared to CeO_2/Si film indicates that extent of interfacial reaction between CeO_2 and Si by means of reduction of Ce^{4+} to Ce^{3+} is less in Pt/CeO_2 thin film deposited on Si substrate.

O1s core level spectra

Oxidation states of Ce in $Pt/CeO_2/Si$ and $Pt/CeO_2/Si_3N_4$ films can also be evaluated from respective O1s core level spectrum. Curve fitted O1s core level spectra from as-deposited $Pt/CeO_2/Si$ and $Pt/CeO_2/Si_3N_4$ films are shown in Fig. 6. Curve fitted O1s core level spectrum in Pt/CeO_2 film on Si contains four component peaks at 529.9, 531.6, 532.6 and 533.6 eV. Peak at 529.9 eV is related to O^{2-} species in CeO_2, whereas peak at 532.6 eV is associated with O in

Si–O bonded species that agrees well with the literature [32,41]. Intermediate peak at 531.6 eV corresponds to Ce^{3+} species originated from silicate or Ce_2O_3 species [32]. Areas under O1s component peaks associated with Ce^{4+} and Ce^{3+} species provide their individual concentrations. It has been estimated that 26% Ce^{3+} species is observed to be present in $Pt/CeO_2/Si$ film which is close to the value obtained from corresponding Ce3d peak. A weak higher binding energy component peak at 533.6 eV is assigned for adsorbed H_2O species [42]. In contrast, an intense peak at 529.9 eV in O1s core level spectrum is observed in $Pt/CeO_2/Si_3N_4$ film that corresponds to O^{2-} species in CeO_2. Two low intense component peaks at 531.5 and 532.5 eV stand for oxygen species in silicate or Ce_2O_3 and Si–O network, respectively. Thus, O1s core levels demonstrate that the relative concentration of Ce^{3+} related oxygen species is highest in the CeO_2/Si film compared to Si_3N_4 substrate.

Si2p core level spectra

Core level Si2p spectra of Si and Si_3N_4 substrates coated with Pt/CeO_2 films are shown in Fig. 7. Broad envelop of Si2p core level spectrum in $Pt/CeO_2/Si$ indicates the presence of several Si species that can be resolved into component peaks. A peak at 99.2 eV is associated with elemental Si present in Si substrate, whereas peaks observed at 101.1 and 102.6 eV correspond to Si^{2+} and Si^{3+} species [43,44]. The presence of these species at the interface of Pt/CeO_2 and Si shows the interaction between them where it can be expected to bond in a Si–Ce–O matrix in the form of silicate [41,45]. On the other hand, a single peak at 101.6 eV in Si2p core level spectrum in $Pt/CeO_2/Si_3N_4$ film is attributed to Si–N bond in Si_3N_4 [46]. It is to be noted that observation of substrate core level signal in these films of 25 nm thickness, especially in the case of reactive substrate like Si indicates the intermixing of Pt/CeO_2 film and Si. Little interfacial reaction occurs in the case of Si_3N_4 substrate as evident from the very weak substrate signal.

Depth profile studies

In order to get the electronic structure and compositions of underneath layers, Pt/CeO_2 films deposited on Si and Si_3N_4 substrates have been mildly sputtered up to few layers and their compositions as well as elemental oxidation states in each interior layers have been analyzed by XPS. Core level spectra of Pt4f and Ce3d of $Pt/CeO_2/Si$ and $Pt/CeO_2/Si_3N_4$ thin films at different stages of sputtering are shown in Fig. 8. Ratios of C_{Pt}/C_{Si}, C_{Ce}/C_{Si} and C_{Pt}/C_{Ce} obtained from depth profiles of $Pt/CeO_2/Si$ and $Pt/CeO_2/Si_3N_4$ films are displayed in Fig. 9. It has been noticed that concentrations of both Pt and Ce get reduced in relation to Si in $Pt/CeO_2/Si$ and $Pt/CeO_2/Si_3N_4$ thin films upon sputtering. In both the cases, films grow layer by layer fashion on the substrates as seen from variation of Pt/Si and Ce/Si concentration ratios with sputtering. However, C_{Pt}/C_{Ce} ratio shows a different behavior at different stages of sputtering. In case of $Pt/CeO_2/Si$ film, the ratio has been observed to decrease up to certain layer and then it increases, whereas it decreases monotonically in $Pt/CeO_2/Si_3N_4$ film. In $Pt/CeO_2/Si$ film, Pt appears to segregate at the interface of Si substrate and film as observed from the C_{Pt}/C_{Ce} ratio in depth profile. In contrast, Pt seems to be diffused outward in case of $Pt/CeO_2/Si_3N_4$ film.

In the present study, there is no diffraction peak related to Pt metal or its oxides in the XRD patterns of Pt/CeO_2 films deposited on Si and Si_3N_4. XPS studies of these films demonstrate that Pt is present as Pt^{2+} and Pt^{4+} oxidation states in the films indicating the incorporation of Pt into CeO_2 matrix that supports XRD results. Our previous studies have shown the significant reduction of Ce^{4+} in CeO_2 into Ce^{3+} in CeO_2/Si film while the reduction is nearly controlled in CeO_2/Si_3N_4 film [30]. In the present work, extent of interaction between CeO_2 and Si is less in $Pt/CeO_2/Si$ film compared to CeO_2/Si film that can be seen in Table 3. Concentration of Ce^{3+} is 32% in CeO_2/Si film, whereas it is 23% in $Pt/CeO_2/Si$ film. It has also

been noticed that concentration of Pt^{2+} is more in $Pt/CeO_2/Si$ film in relation to $Pt/CeO_2/Si_3N_4$ film. Stabilization of Pt^{2+} and Pt^{4+} ions in CeO_2 matrix and difference in extent of interfacial reaction can be substantiated from the relative positions of valence bands. Pt metal has high electron density at the Fermi level (E_F) and its valence band extend even up to 6 eV below E_F. On the other hand, valence bands of Si^0, $Ce^{4+}4f$ and Si_3N_4 are 1.1, 2 and 5.1 eV, respectively with respect to Fermi level [12,47,48]. Therefore, Pt can transfer its electrons easily to Ce^{4+} that facilitates conversion of Ce^{4+} to Ce^{3+} to a certain extent and Pt itself can be oxidized to form Pt^{2+} and Pt^{4+}. Again, Pt can also give electrons to Si^0 that can sluggish the interaction between CeO_2 and Si. Therefore, internal electron transfer among Pt, CeO_2 and Si results in the formation of Pt^{2+} and Pt^{4+} in $Pt/CeO_2/Si$ film. In contrast, this type of electron transfer cannot be facilitated in $Pt/CeO_2/Si_3N_4$ film as valence band level of Si_3N_4 is located in lower energy side in relation to Pt^0 and Ce^{4+} according to the Fermi level. Moreover, Si_3N_4 is an inert substrate as it has filled p levels of Si. In this sense, synergistic interaction mainly occurs between Pt and CeO_2 in $Pt/CeO_2/Si_3N_4$ film. Here, Pt transfers its electrons to CeO_2 only leading to the formation of more Pt^{4+} species. Therefore, concentration of Ce^{3+} species is observed to be more in $Pt/CeO_2/Si_3N_4$ film compared to CeO_2/Si_3N_4 film. It is important to note that there can be a possibility of formation of platinum silicide phase in $Pt/CeO_2/Si$ film thermodynamically at room temperature [49,50]. However, in the present study, platinum silicide formation has not been observed as evident from core level binding energy of Si2p core level.

4. Conclusions

Pt/CeO_2 films were deposited on Si and Si_3N_4 substrates by magnetron sputtering. XRD patterns confirm the presence of nanocrystalline CeO_2 phase on Si and Si_3N_4 substrates. XPS studies show the presence of Pt^{2+} as predominant species in $Pt/CeO_2/Si$ film, whereas Pt^{4+}

concentration is observed to be more in $Pt/CeO_2/Si_3N_4$ film. There is no signature of Pt metal peak in XRD patterns indicating the incorporation of Pt into CeO_2 lattice as ions. Extent of interaction between CeO_2 and Si is less in presence of Pt in $Pt/CeO_2/Si$ film. Depth profiling studies show that Pt is segregating at the Si/film interface in $Pt/CeO_2/Si$ film and Pt is diffusing outwards in $Pt/CeO_2/Si_3N_4$ film.

Acknowledgments

Authors would like to thank the Director, CSIR–National Aerospace Laboratories for giving permission to publish this work. Authors wish to acknowledge Mr. Siju and Mr. Praveen for carrying out FESEM and AFM measurements, respectively.

References

[1] S.D. Jackson, J.S.J. Hargreaves, Eds. Metal Oxide Catalysis, Wiley–VCH, Weinheim, Germany, 2009.

[2] M. Fernández-García, A. Martínez-Arias, J.C. Hanson, J.A. Rodriguez, Chem. Rev. 104 (2004) 4063.

[3] X. Chen, S.S. Mao, Chem. Rev. 107 (2007) 2891.

[4] J. Jiang, Y. Li, J. Liu, X. Huang, C. Yuan, X.W. Lou, Adv. Mater. 24 (2012) 5166.

[5] G. Korotcenkov, Mater. Sci. Eng. B 139 (2007) 1.

[6] M.M. Arafat, B. Dinan, S.A. Akbar, A.S.M.A. Haseeb, Sensors, 12 (2012) 7207.

[7] S. Chen, J. R. Manders, S.-W. Tsang, F. So, J. Mater. Chem. 22 (2012) 24202.

[8] H. Huang, B. Liang, Z. Liu, X. Wang, D. Chen, G. Shen, J. Mater. Chem. 22 (2012) 13428.

[9] E. Fortunato, P. Barquinha, R. Martins, Adv. Mater. 24 (2012) 2945.

[10] J. Meyer, S. Hamwi, M. Kröger, W. Kowalsky, T. Riedl, A. Kahn, Adv. Mater. 24 (2012) 5408.

[11] A. Trovarelli, Catalysis by Ceria and Related Materials, Imperial College Press, London, 2002.

[12] P. Bera, M.S. Hegde, Catal. Surv. Asia 15 (2011) 181.

[13] P. Bera, M.S. Hegde, J. Indian Inst. Sci. 90 (2010) 299.

[14] C.-S. Oh, C.-I. Kim, K.-H. Kwon, J. Vac. Sci. Technol. A 19 (2001) 1068.

[15] F.-C. Chiu, C.-M. Lai, J. Phys. D: Appl. Phys. 43 (2010) 075104.

[16] M. Mogensen, N.M. Sammes, G.A. Tompsett, Solid State Ionics 129 (2000) 63.

[17] H. Inaba, H. Tagawa, Solid State Ionics 83 (1996) 1.

[18] M.R. Mohammadi, D.J. Fray, Sens. Actuator B 150 (2010) 631.

[19] X. Zhong, Q. Li, J. Hu, Y. Lu, Corros. Sci. 50 (2008) 2304.

[20] P. Bera, K.C. Patil, V. Jayaram, G.N. Subbanna, M.S. Hegde, J. Catal. 196 (2000) 293.

[21] M.A. Scibioh, S.-K. Kim, E.A. Cho, T.-H. Lim, S.-A. Hong, H.Y. Ha, Appl. Catal. B 84 (2008) 773.

[22] M. Václavů, I. Matolínová, J. Mysliveček, R. Fiala, V. Matolín, J. Electrochem. Soc. 156 (2009) B938.

[23] V. Matolín, I. Matolínová, M. Václavů, I. Khalakhan, M. Vorokhta, R. Fiala, I. Piš, Z. Sofer, J. Poltierová-Vejpravová, T. Mori, V. Potin, H. Yoshikawa, S. Ueda, K. Kobayashi, Langmuir 26 (2010) 12824.

[24] V. Matolín, I. Khalakhan, I. Matolínová, M. Václavů, K. Veltruská, M. Vorokhta, Surf. Interface Anal. 42 (2010) 882.

[25] M. Vorokhta, I. Khalakhan, I. Matolínová, M. Kobata, H. Yoshikawa, K. Kobayashi, V. Matolín, Appl. Surf. Sci. 267 (2013) 119.

[26] I. Khalakhan, M. Dubau, S. Haviar, J. Lavková, I. Matolínová, V. Potin, M. Vorokhta, V. Matolín, Ceram. Int. 39 (2013) 3765.

[27] I. Matolínová, R. Fiala, I. Khalakhan, M. Vorokhta, Z. Sofer, H. Yoshikawa, K. Kobayashi V. Matolín, Appl. Surf. Sci. 258 (2012) 2161.

[28] H.-J. Ahn, J.-S. Jang, Y.E. Sung, T.-Y. Seong, J. Alloys Compd. 473 (2009) L28.

[29] V. Fernandes, I.L. Graff, J. Varalda, L. Amaral, P. Fichtner, D. Demaille, Y. Zheng, W.H. Schreiner, D.H. Mosca, J. Electrochem. Soc. 159 (2012) K27.

[30] C. Anandan, P. Bera, Appl. Surf. Sci. 283 (2013) 297.

[31] P. Bera, C. Anandan, Surf. Rev. Lett. (DOI:10.1142/S0218625X14500541).

[32] F. Pagliuca, P. Luches, S. Valeri, Surf. Sci. 607 (2013) 164.

[33] L. Kim, J. Kim, D. Jung, C.-Y. Park, C.-W. Yang, Y. Roh, Thin Solid Films 360 (2000) 154.

[34] R. Rangel, L. Chávez-Chávez, E. Martínez, P. Bartolo-Pérez, Phys. Status Solidi B 249 (2012) 1199.

[35] P. Bera, K.R. Priolkar, A. Gayen, P.R. Sarode, M.S. Hegde, S. Emura, R. Kumashiro, V. Jayaram, G.N. Subbanna, Chem. Mater. 15 (2003) 2049.

[36] P. Bera, A. Gayen, M.S. Hegde, N.P. Lalla, L. Spadaro, F. Frusteri, F. Arena, J. Phys. Chem. B 107 (2003) 6122.

[37] V. Fernandes, I.L. Graff, J. Varalda, L. Amaral, P. Fichtner, D. Demaille, Y. Zheng, W.H. Schreiner, D.H. Mosca, J. Electrochem. Soc. 159 (2012) K27.

[38] D.R. Mullins, S.H. Overbury, D.R. Huntley, Surf. Sci. 409 (1998) 307.

[39] E. Beche, G. Peraudeau, V. Flaud, D. Perarnau, Surf. Interface Anal. 44 (2012) 1045.

[40] E.J. Preisler, O.J. Marsh, R.A. Beach, T.C. McGill, J. Vac. Sci. Technol. B 19 (2001) 1611.

[41] T. Skála, V. Matolín, Appl. Surf. Sci. 265 (2013) 817.

[42] P. Bera, H. Seenivasan, K.S. Rajam, C. Shivakumara, S.K. Parida, Surf. Interface Anal. 45 (2013) 1026.

[43] G. Hollinger, F.J. Himpsel, Appl. Phys. Lett. 44 (1984) 93.

[44] J.R. Shallenberger, J. Vac. Sci. Technol. A 14 (1996) 693.

[45] R. Barnes, D. Starodub, T. Gustafsson, E. Garfunkel, J. Appl. Phys. 100 (2006) 044103.

[46] S.I. Raider, R. Flitsch, J.A. Aboaf, W.A. Pliskin, J. Electrochem. Soc. 123 (1976) 560.

[47] A. Bahari, P. Morgen, Z.S. Li, Surf. Sci. 600 (2006) 2966.

[48] C. Sénémaud, M. Driss-Khodja, A. Gheorghiu, S. Harel, G. Dufour, H. Roulet, J. Appl. Phys. 74 (1993) 5042.

[49] G. Larrieu, E. Dubois, X. Wallart, X. Baie, J. Katcki, J. Appl. Phys. 94 (2003) 7801.

[50] J. Yin, W. Cai, Y. Zheng, L. Zhao, Surf. Coat. Technol. 198 (2005) 329.

Table 1. Binding energies, FWHMs and integrated peak areas of $Ce3d_{5/2,3/2}$ spin-orbit doublets in Pt/CeO_2 film deposited on Si.

Peak assignment	Ce species	Binding energy peak (eV)	Relative area (%)
v_0	Ce^{3+}	881.7	6
v	Ce^{4+}	882.5	13
v′	Ce^{3+}	885.3	8
v″	Ce^{4+}	888.5	13
v‴	Ce^{4+}	897.9	16
u_0	Ce^{3+}	899.1	4
u	Ce^{4+}	900.9	10
u′	Ce^{3+}	903.4	5
u″	Ce^{4+}	907.0	11
u‴	Ce^{4+}	916.4	14

Table 2. Binding energies, FWHMs and integrated peak areas of $Ce3d_{5/2,3/2}$ spin-orbit doublets in Pt/CeO_2 film deposited on Si_3N_4.

Peak assignment	Ce species	Binding energy peak (eV)	Relative area (%)
v_0	Ce^{3+}	881.7	4
v	Ce^{4+}	882.6	14
v′	Ce^{3+}	885.2	6
v″	Ce^{4+}	888.3	16
v‴	Ce^{4+}	897.9	17
u_0	Ce^{3+}	899.2	3
u	Ce^{4+}	901.0	11
u′	Ce^{3+}	903.3	4
u″	Ce^{4+}	907.2	12
u‴	Ce^{4+}	916.4	13

Table 3. Relative surface concentrations of Ce^{4+} and Ce^{3+} components evaluated from XPS in Pt/CeO_2 and CeO_2 thin films deposited on Si and Si_3N_4 substrates.

Thin films	Ce^{4+}	Ce^{3+}
$Pt/CeO_2/Si$	77	23
CeO_2/Si	68	32
$Pt/CeO_2/ Si_3N_4$	83	17
CeO_2/Si_3N_4	89	11

Figure captions

Fig. 1. XRD patterns of Pt/CeO_2 thin films deposited on (a) Si and (b) Si_3N_4 substrates.

Fig. 2. FESEM images of Pt/CeO_2 thin films deposited on (a) Si and (b) Si_3N_4 substrates.

Fig. 3. AFM images of Pt/CeO_2 thin films deposited on (a) Si and (b) Si_3N_4 substrates.

Fig. 4. Curve fitted XPS of Pt4f core levels of Pt/CeO_2 thin films deposited on (a) Si and (b) Si_3N_4 substrates.

Fig. 5. Curve fitted XPS of Ce3d core levels of Pt/CeO_2 thin films deposited on Si and Si_3N_4 substrates.

Fig. 6. Curve fitted XPS of O1s core levels in as-deposited Pt/CeO_2 thin films on (a) Si and (b) Si_3N_4 substrates.

Fig. 7. Curve fitted XPS of Si2p core levels of Pt/CeO_2 thin films deposited on Si and Si_3N_4 substrates.

Fig. 8. XPS of Ce3d and Pt4f core levels of $Pt/CeO_2/Si$ (top) and $Pt/CeO_2/Si_3N_4$ (bottom) thin films with different stages of sputtering: (a) as-deposited, (b) 3 min, (c) 8 min, (d) 13 min, (e) 18 min, (f) 23 min and (g) 28 min.

Fig. 9. C_{Pt}/C_{Si}, C_{Ce}/C_{Si} and C_{Pt}/C_{Ce} ratios in $Pt/CeO_2/Si$ and $Pt/CeO_2/Si_3N_4$ films as function of sputtering time.

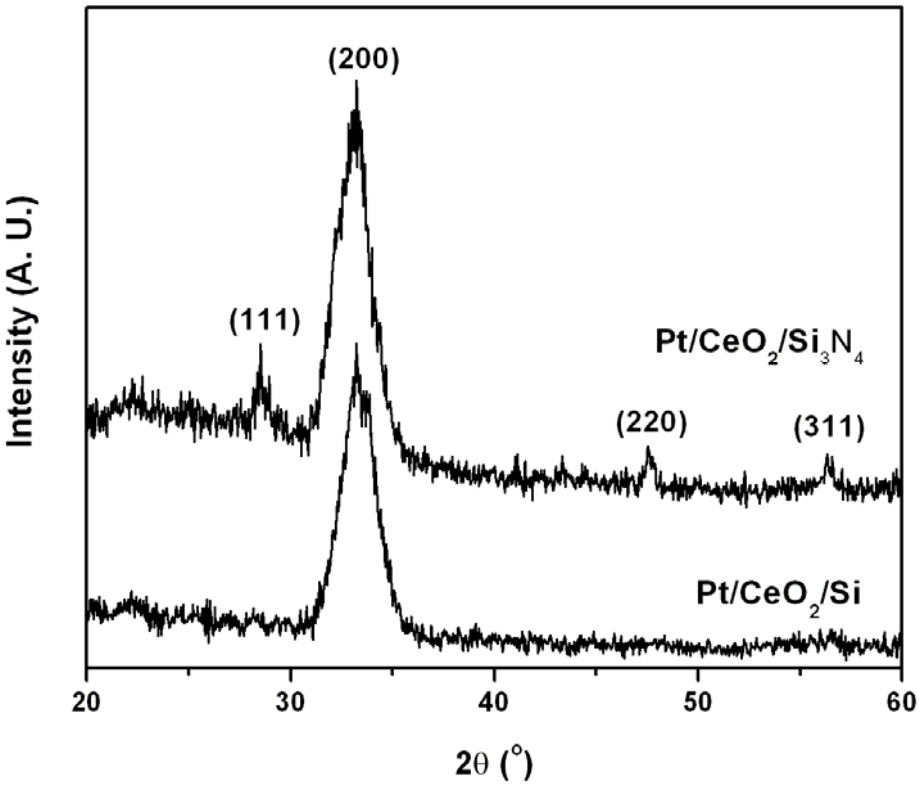

Fig. 1. XRD patterns of $Pt/CeO_2/Si$ and $Pt/CeO_2/Si_3N_4$ thin films.

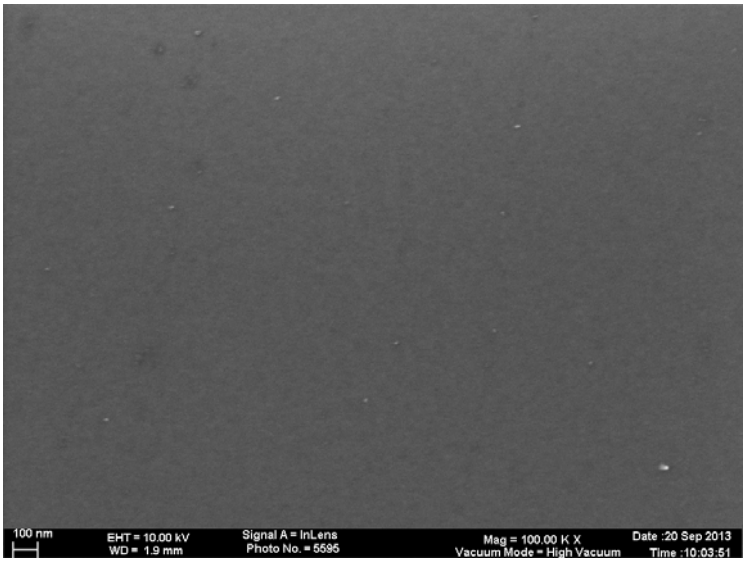

$Pt/CeO_2/Si$

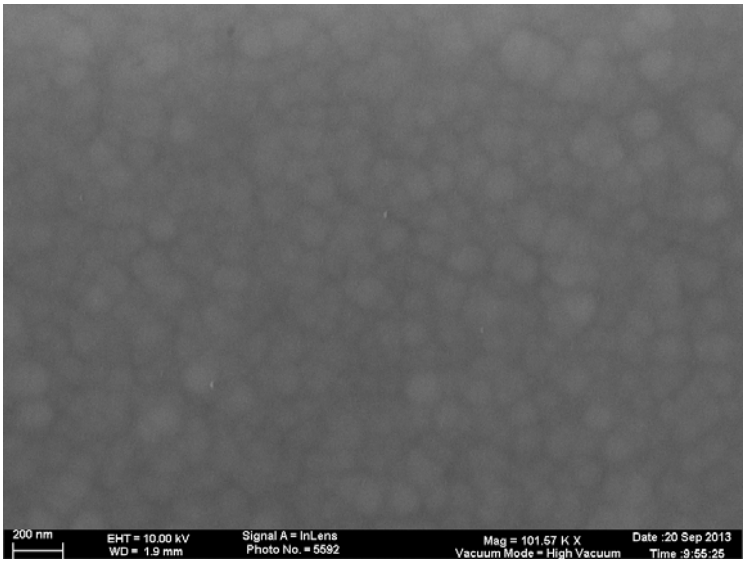

$Pt/CeO_2/Si_3N_4$

Fig. 2. FESEM images of $Pt/CeO_2/Si$ and $Pt/CeO_2/Si_3N_4$ thin films.

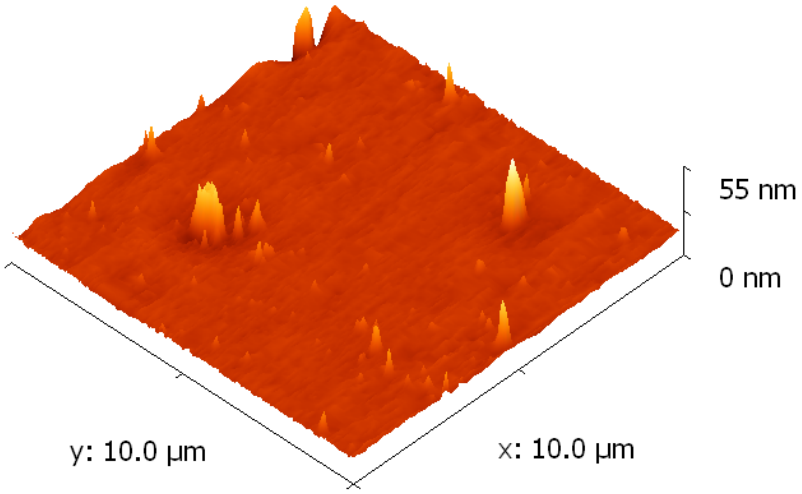

Pt/CeO_2/Si

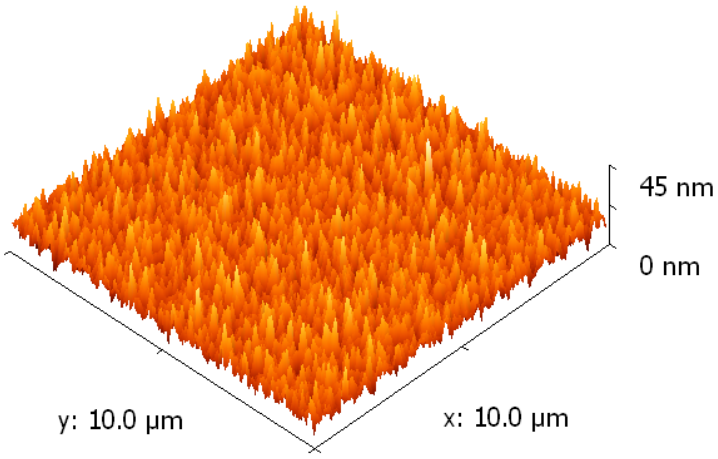

Pt/CeO_2/Si_3N_4

Fig. 3. AFM images of Pt/CeO_2/Si and Pt/CeO_2/Si_3N_4 thin films.

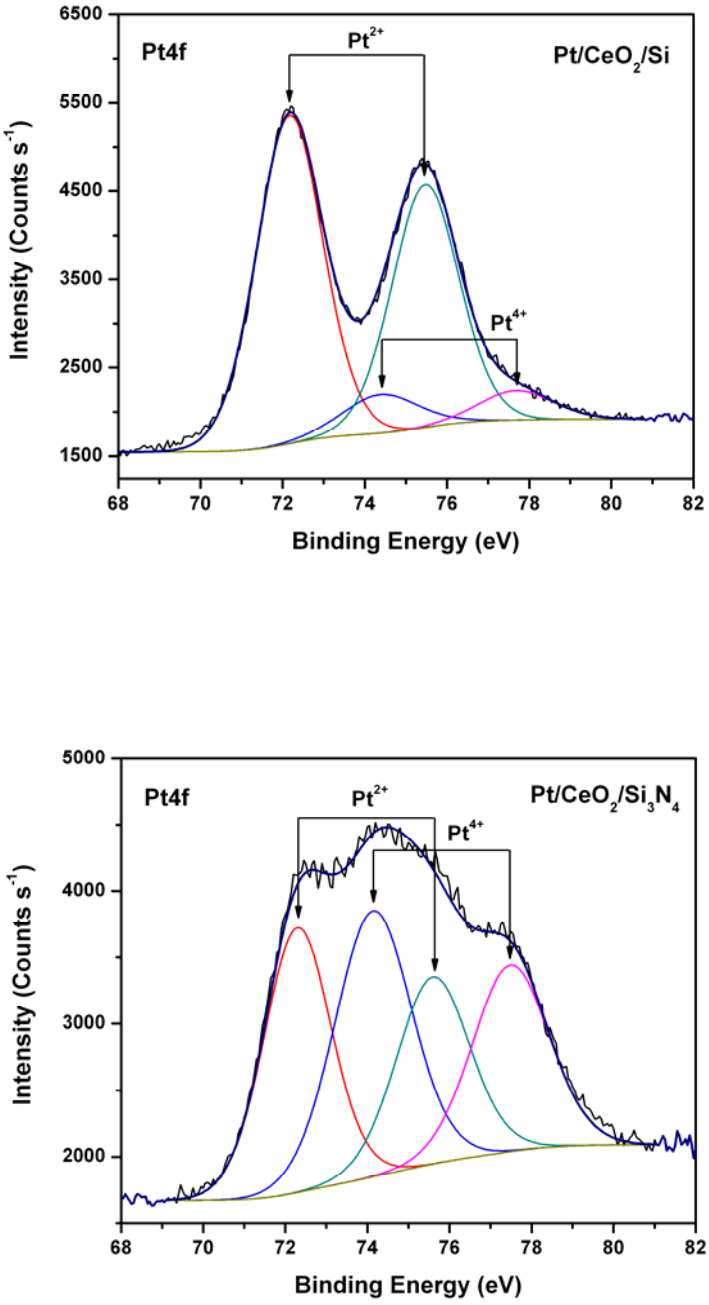

Fig. 4. Curve fitted XPS of Pt4f core levels of $Pt/CeO_2/Si$ and $Pt/CeO_2/Si_3N_4$ thin films.

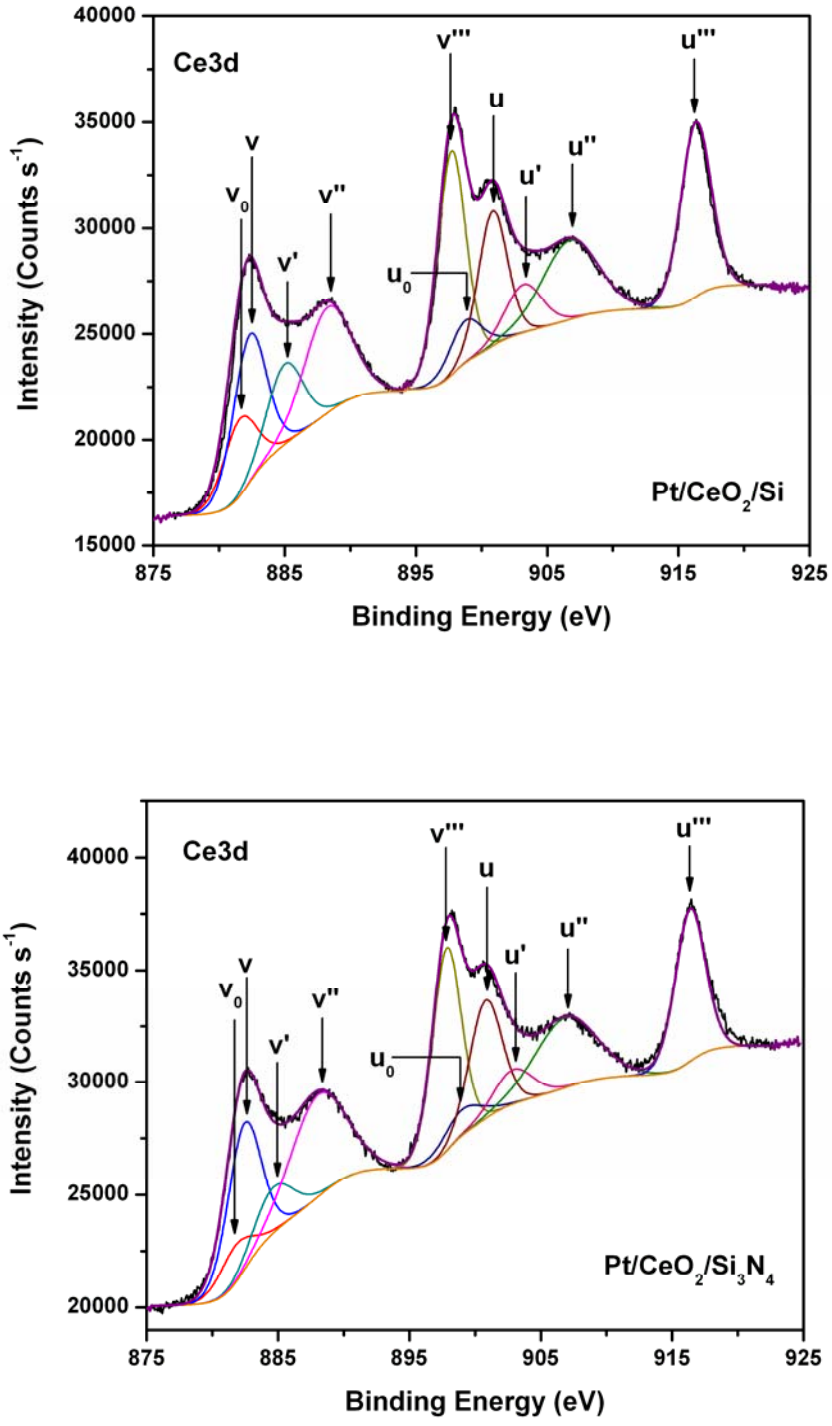

Fig. 5. Curve fitted XPS of Ce3d core levels of $Pt/CeO_2/Si$ and $Pt/CeO_2/Si_3N_4$ thin films.

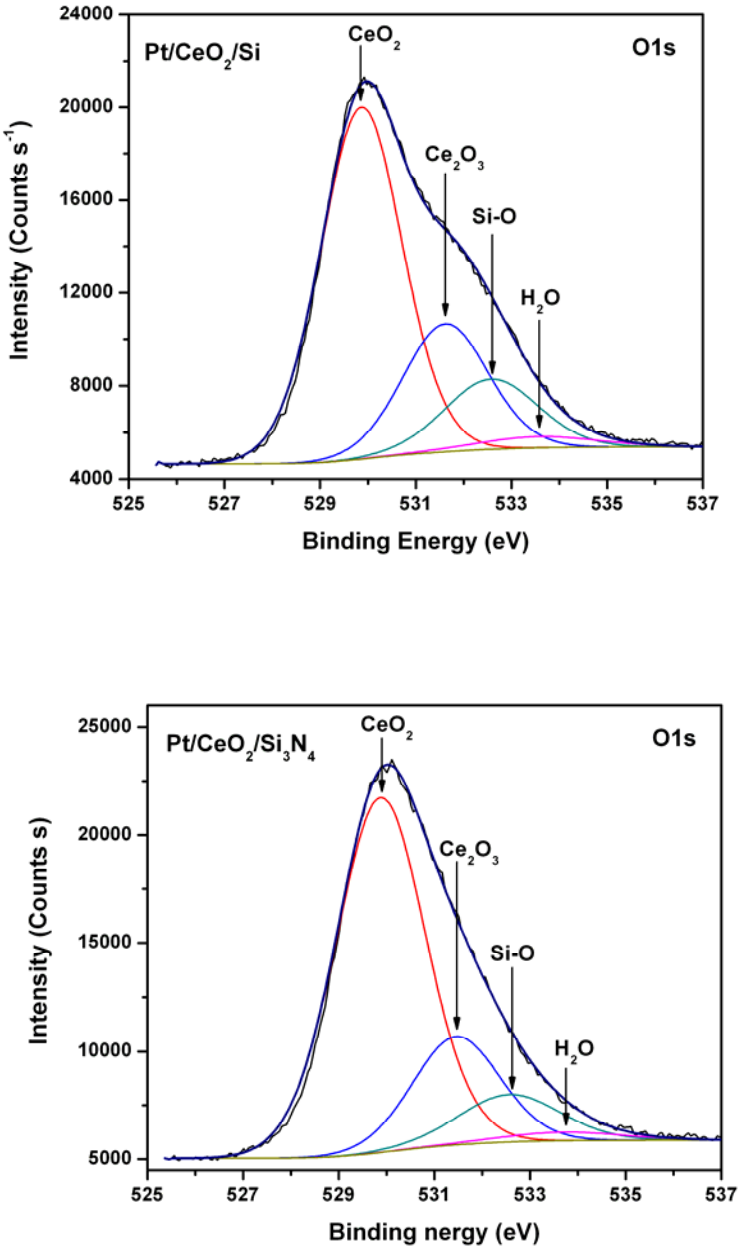

Fig. 6. Curve fitted XPS of O1s core levels in $Pt/CeO_2/Si$ and $Pt/CeO_2/Si_3N_4$ thin films.

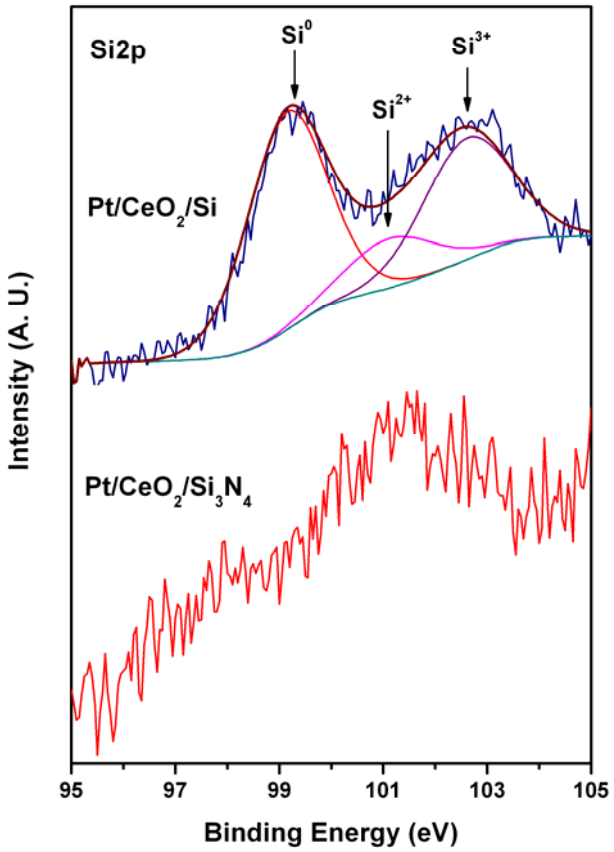

Fig. 7. Curve fitted XPS of Si2p core levels of $Pt/CeO_2/Si$ and $Pt/CeO_2/Si_3N_4$ thin films.

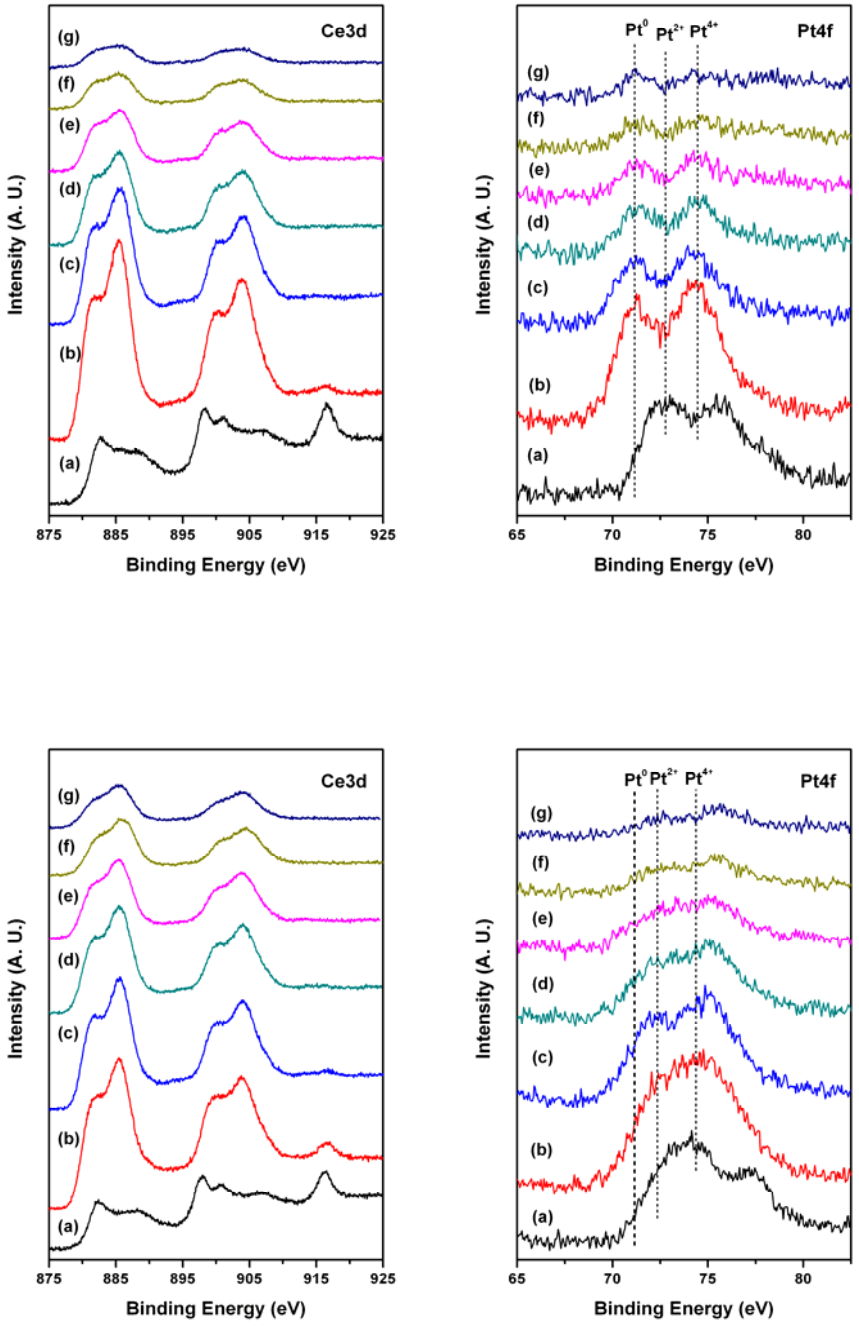

Fig. 8. XPS of Ce3d and Pt4f core levels of Pt/CeO_2/Si (top) and Pt/CeO_2/Si_3N_4 (bottom) thin films with different stages of sputtering: (a) as-deposited, (b) 3 min, (c) 8 min, (d) 13 min, (e) 18 min, (f) 23 min and (g) 28 min.

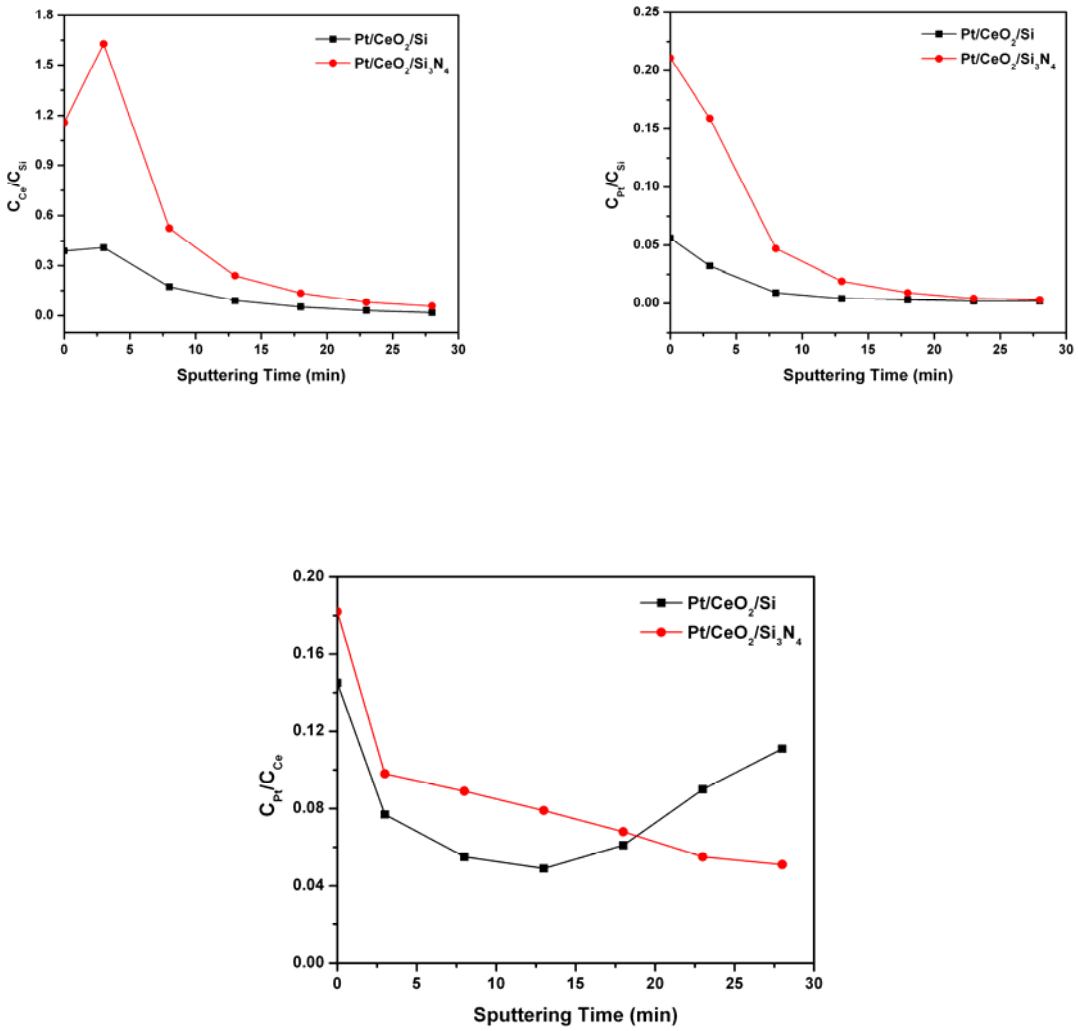

Fig. 9. C_{Pt}/C_{Si}, C_{Ce}/C_{Si} and C_{Pt}/C_{Ce} ratios in $Pt/CeO_2/Si$ and $Pt/CeO_2/Si_3N_4$ films as function of sputtering time.